scientific reports

Check for updates

OPEN

Synthesis of trimetallic oxide (Fe_2O_3–MgO–CuO) nanocomposites and evaluation of their structural and optical properties

A. H. Al-Hammadi[1], Adnan Alnehia[1,2], Annas Al-Sharabi[2], Hisham Alnahari[1]✉ & Abdel-Basit Al-Odayni[3]

In this paper, tri-phase Fe_2O_3–MgO–CuO nanocomposites (NCs) and pure CuO, Fe_2O_3 and MgO nanoparticles (NPs) were prepared using sol–gel technique. The physical properties of the prepared products were examined using SEM, XRD, and UV–visible. The XRD data indicated the formation of pure CuO, Fe_2O_3 and MgO NPs, as well as nanocomposite formation with Fe_2O_3 (cubic), MgO (cubic), and CuO (monoclinic). The crystallite size of all the prepared samples was calculated via Scherrer's formula. The energy bandgap of CuO, Fe_2O_3 and MgO and Fe_2O_3–MgO–CuO NCs were computed from UV–visible spectroscopy as following 2.13, 2.29, 5.43 and 2.96 eV, respectively. The results showed that Fe_2O_3–MgO–CuO NCs is an alternative material for a wide range of applications as optoelectronics devices due to their outstanding properties.

Due to their unique optical, electrical, thermal, photocatalytic, mechanical, adsorbent and structural properties, metal oxide (MO) nanocomposites (NCs) have attracted much attention in recent years[1–5]. The NCs are composed of two or more nano-oxides and possessing properties which depend on the concentration of each constituent oxide in the mixture[6–8]. They are useful in a variety of applications, including solar cells, photovoltaic instruments, battery materials, gas sensors, and fuel cells[9–15]. Copper oxide (CuO) is a p-type semiconductor with a narrow bandgap of 1.2 eV[8]. It has unique optical and structural properties with low-cost preparation. It has attracted considerable attention due to its potential applications in superconductivity, gas sensing, solar cell and supercapacitor[16,17]. Furthermore, it is a non-toxic and readily available semiconductor[18,19]. Magnesium oxide (MgO), with a direct bandgap of 5.2–7 eV, is an n-type semiconductor that displays noticeable structural, catalytic, optical, and chemical properties[17,20–22]. Iron(III) oxide (Fe_2O_3) is a narrow bandgap of nearly 2 eV. It is associated with certain features, like the low toxicity, low cost, magnetic behavior and high solubility[23,24]. Hence, it is engaged in various applications involving biomedicine, cosmetics, diagnostics, sensors, radiology, and vaccines[9,23,25,26].

By combining the different metal oxides (MOs) to form new NCs, various properties of individual oxide could significantly enhanced and, consequently, open up a new avenue of research for optoelectronics, electrical, thermal, photo-catalysis, and biological applications[26,27]. Mixed metal oxide NCs can be fabricated via different approaches such as the co-precipitation[28], sonochemical[7], solution combustion[29], microwave technique[10], ultrasonic-assisted[30] and green methods[2,11].

In this work, tri-phase Fe_2O_3–MgO–CuO NCs and pure CuO, Fe_2O_3 and MgO NPs were prepared using sol–gel method. It has the advantages of being environmentally friendly, simple, cheap and fast to perform without any special equipment. Herein, the novelty lies in the designed combination of the three metal oxides in one NC, which supposedly could lead to enhanced properties and potential applications. The obtained oxides were characterized for their structural and optical properties using XRD, UV–visible, and SEM.

[1]Department of Physics, Faculty of Sciences, Sana'a University, Sana'a 12081, Yemen. [2]Department of Physics, Faculty of Applied Sciences, Thamar University, Dhamar 87246, Yemen. [3]Engineer Abdullah Bugshan Research Chair for Dental and Oral Rehabilitation, College of Dentistry, King Saud University, 11545 Riyadh, Saudi Arabia. ✉email: his.alnahari@su.edu.ye

Materials and methods

Materials. Magnesium nitrate hexahydrate ($Mg(NO_3)_2{\cdot}6H_2O$; 97%), Iron nitrate nonahydrate ($Fe(NO_3)_3{\cdot}9H_2O$; 97%), copper nitrate trihydrate ($Cu(NO_3)_2{\cdot}3(H_2O$; 98%) and absolute ethanol were purchased from BDH and used as received without additional treatment.

Synthesis. The sol–gel method[20,31] was used to fabricate the Fe_2O_3–MgO–CuO NCs, which involves the following steps: $Cu(NO_3)_2{\cdot}3(H_2O)$ (3.382 g in 20 mL ethanol), $Fe(NO_3)_3{\cdot}9(H_2O)$ (5.65 g in 20 mL ethanol) and $Mg(NO_3)_2{\cdot}6(H_2O)$ (3.589 g in 20 mL ethanol) with constant molar ratio (1:1:1) were synthesized as three separate solutions. Each solution was stirred for 10 min at 23 ± 2 °C to obtain a homogeneous solution. The solutions were mixed under constant stirring for 70 min at 80 °C until gel was obtained. After that, the gel burns to create xerogel, which grinded to fine powder and annealed at 800 °C for 90 min. The individual pure oxides (Fe_2O_3, CuO, and MgO) were separately prepared following similar steps as composite, using the corresponding salt.

Instruments. The optical properties of the synthesized materials were investigated using UV–Vis spectrophotometer (Hitachi U3900 with a software of Varian Cary 50). The structural properties were investigated by X-ray diffraction (XRD) using a Shimadzu EDX-720 (China) with CuKα radiation (λ = 0.154 nm). Morphological properties were assessed using SEM machine from JEOL (Jeol Ltd., Tokyo, Japan).

Results and discussion

The structural integrity of the synthesized metal oxides is confirmed via powder X-ray crystallography. The targeted substances were obtained via sol–gel route followed by calcination at 800 °C. The annealing temperature of 800 °C suggests high crystalline products as reported elsewhere[32]. However, such high temperature could stimulate production of pure substances with better performance.

X-ray diffraction. The crystalline arrangements and phase of the prepared nanopowder are estimated by XRD. Figure 1 shows the XRD pattern of the fabricated Fe_2O_3–MgO–CuO NCs. The observed diffraction peaks of pure oxides are close to the diffraction patterns reported in the X-ray database of JCPDS CuO (45-0937), Fe_2O_3 (33-0664) and MgO (45-0946). Similarly, in Fe_2O_3–MgO–CuO NCs, the diffraction patterns of CuO (48-1548), Fe_2O_3 (39-1346), and MgO (45-0946) match well with their respective standard reference cards. The

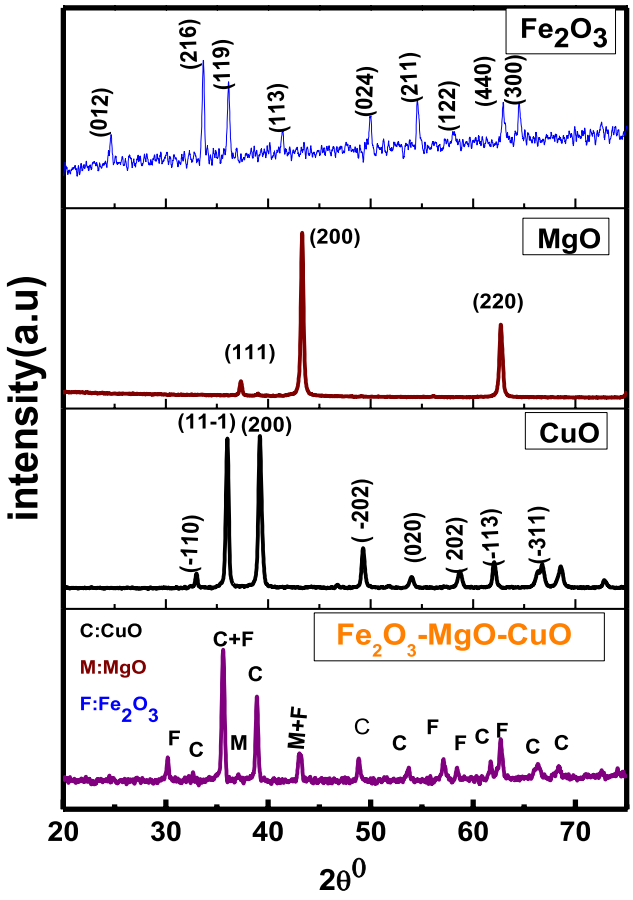

Figure 1. XRD patterns of CuO, Fe_2O_3, MgO and Fe_2O_3–MgO–CuO nanocomposites.

diffracted peaks in composite were assigned for MgO (cubic), Fe_2O_3 (cubic) and CuO (monoclinic) phases. The characteristic diffraction peaks of CuO, Fe_2O_3 and MgO are well specified with no peaks relating to secondary or impurity segments or hydroxide in the sample, confirming the successful growth of Fe_2O_3–MgO–CuO NCs. The crystalline nature of the sample is assessed based on the sharp and strong diffraction peaks in Fig. 1. The cell volume (v), lattice constants (a, b, c) and d-spacing for pure CuO monoclinic, MgO cubic and Fe_2O_3 hexagonal phase and Fe_2O_3–MgO–CuO nanocomposite were calculated[22,33–36] and listed in Table 1.

The Scherrer equation[37] was utilized to compute the crystallite size (D) of CuO, Fe_2O_3, MgO and Fe_2O_3–MgO–CuO NCs. Then, their dislocation density was also calculated[1,38,39], Table 2. As can be seen, the average D values of CuO, and MgO were larger than in the NCs as compared with individual oxides, due to the agglomeration of particles caused by the presence of Fe_2O_3. The Fe_2O_3 particles act as nucleation sites for the CuO and MgO particles, resulting in aggregation into larger clusters. This phenomenon is known as the Ostwald ripening effect, where smaller particles dissolve and re-deposit on larger particles, resulting in an increase in their size. Hence, the presence of Fe_2O_3 in the NCs leads to an increase in the particle size of CuO and MgO.

SEM analysis. Figure 2 represents the SEM images of grown pure CuO, Fe_2O_3, MgO and Fe_2O_3–MgO–CuO NCs. It is seen that the formed nanostructures have spherical shapes with hardly distinct morphology. Furthermore, due to the low resolution of the presented SEM images, the non-size and thus, particle sizes and distribution are difficult to be counted. Nevertheless, the XRD data supported the claimed nanostructures. To improve the seen, and thus the suggested nanostructures, a higher magnification of the SEM image was presented as an insert within the corresponding image. The resulting magnified view is simply support that the particles are in nanometer range. In addition, some nanoparticles are well separated and thus could be counted. For example, by counting of the obviously countable particles of the composite image (Fig. 2D), it is found that the averaged particle size is 153 ± 30 nm, which is higher than that calculated from XRD (56 ± 4 nm) shown in Table 2. According to literature[40,41], the SEM-based particle size is often larger than those measured by other techniques like XRD, the case that can be seen herein.

UV–Vis spectroscopy. The optical properties of the Fe_2O_3–MgO–CuO NCs were studied by UV–visible spectroscopy. Figure 3 displays the absorption spectrum of Fe_2O_3–MgO–CuO NCs within 200–1000 nm. The absorption spectrum of the scattering radiation is observed in the longer wavelength region, and a larger-tail is seen due to the mixing of different oxides.

The transmission spectra of all the synthesized materials showed almost an opposite behavior to that seen in Fig. 4. Obviously, the optical transmission increased in the visible region for all the synthesized materials and possesses maximum value for Fe_2O_3–MgO–CuO NCs. The absorption coefficient (α) value can be computed via the following equation $\alpha = \frac{2.303A}{t}$[34].

The change in α (λ) for CuO, Fe_2O_3, MgO and Fe_2O_3–MgO–CuO NCs is presented in Fig. 5. From this Figure, it can be seen that α decreases as the wavelength (λ) of the incident photon increases. The extinction coefficient (α) value can be calculated via the following equation $k = \frac{\alpha\lambda}{4\pi}$[42,43].

Material	Oxide	ID phase	a (Å)	b (Å)	c (Å)	Volume (Å^3)	d-spacing (Å)
Pure oxides (CuO, Fe_2O_3, MgO)	CuO	Monoclinic	4.685	3.426	5.130	82.3	1.875
	Fe_2O_3	Hexagonal	5.036	5.036	13.749	301.9	1.966
	MgO	Cubic	4.211	4.211	4.211	74.7	1.992
Nanocomposite (CuO–Fe_2O_3–MgO)	CuO	Monoclinic	4.688	3.423	5.132	81.2	2.523
	Fe_2O_3	Cubic	8.351	8.351	8.351	582.4	2.521
	MgO	Cubic	4.211	4.211	4.211	74.7	2.099

Table 1. Geometric parameters of CuO, Fe_2O_3 and MgO in grown Fe_2O_3–MgO–CuO nanocomposites determined from XRD analysis.

Material	Oxide	Average crystallite size (nm)	Average dislocation density (lines/m^2) × 10^{14}
Pure (CuO, Fe_2O_3, MgO)	CuO	22.110	20.456
	Fe_2O_3	89.141	1.258
	MgO	30.120	11.022
Nanocomposite (CuO–Fe_2O_3–MgO)	CuO	51.457	3.777
	Fe_2O_3	55.954	3.194
	MgO	60.305	2.749

Table 2. Structural parameters of CuO, Fe_2O_3 and MgO in grown Fe_2O_3–MgO–CuO nanocomposites determined from XRD analysis.

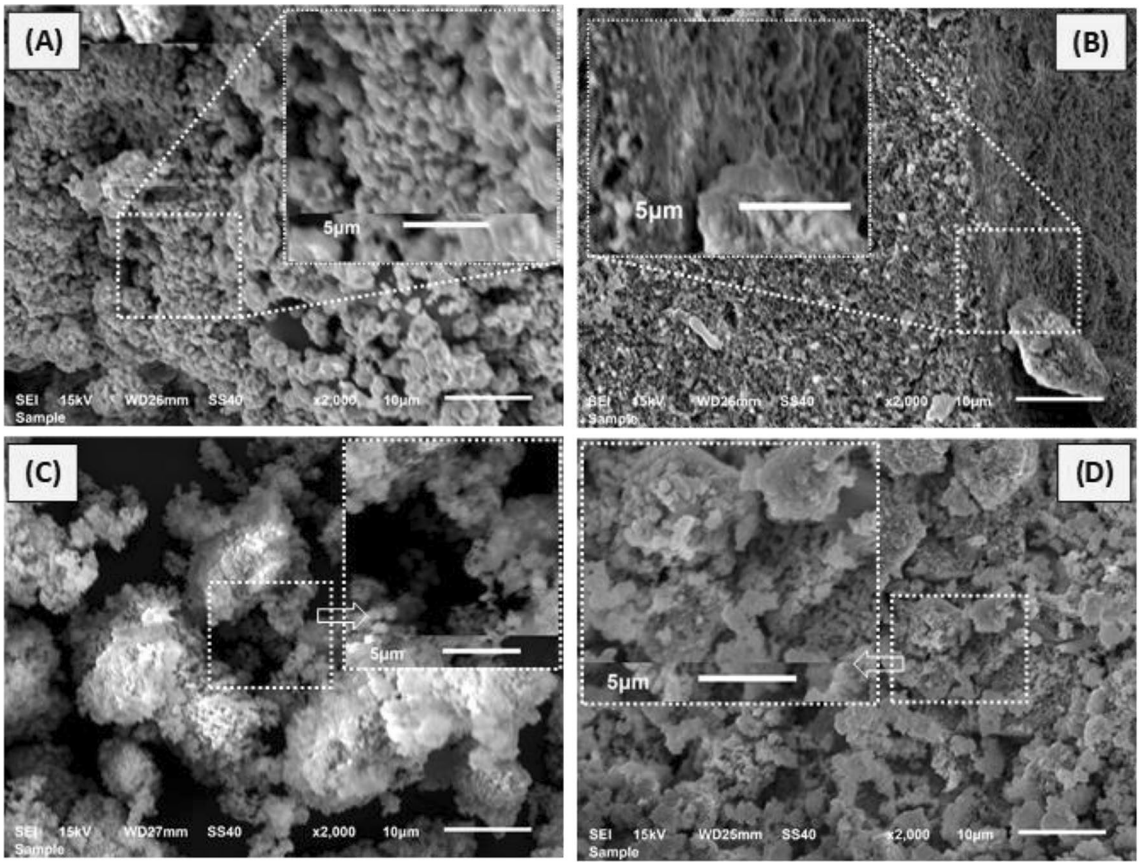

Figure 2. SEM images of (**A**) CuO, (**B**) Fe_2O_3, (**C**) MgO, (**D**) Fe_2O_3–MgO–CuO nanocomposites. Inserts are magnification of the shown selected area.

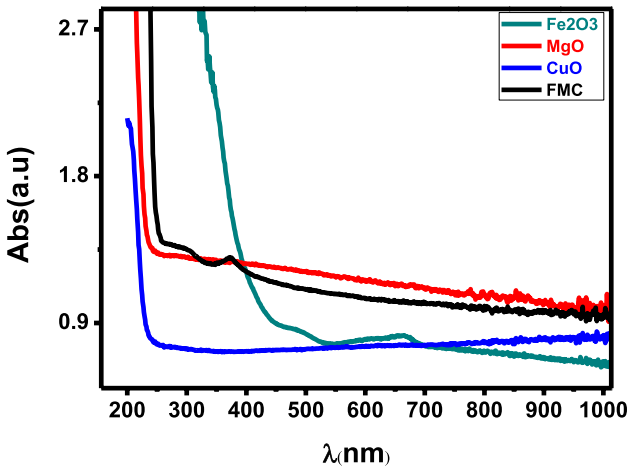

Figure 3. Absorption spectra of CuO, Fe_2O_3, MgO and Fe_2O_3–MgO–CuO (FMC) nanocomposites.

The change in k (λ) for CuO, Fe_2O_3, MgO and Fe_2O_3–MgO–CuO NCs is presented in Fig. 6. It can be observed that k increases as the wavelength of the incident photon increases.

The energy bandgap (Eg) values of CuO, Fe_2O_3, MgO and Fe_2O_3–MgO–CuO NCs for the direct electronic transition between the valence band (VB) and conduction band (CB) can be computed via Tauc's relation[38,44,45] as shown in Fig. 7. The E_g values of CuO, Fe_2O_3, MgO NPs were calculated to about 2.13, 2.29, and 5.43 eV, respectively. However, Fe_2O_3–MgO–CuO NCs displayed the E_g of 2.96 eV. In comparison to individual CuO, Fe_2O_3, MgO NPs, Fe_2O_3–MgO–CuO displayed significant increased absorbance in the visible region due to incorporation of three metal oxide. The reason for the change in the bandgap energy of the NCs compared to the individual metal oxides is likely due to the formation of new energy states at the interfaces between the different metal

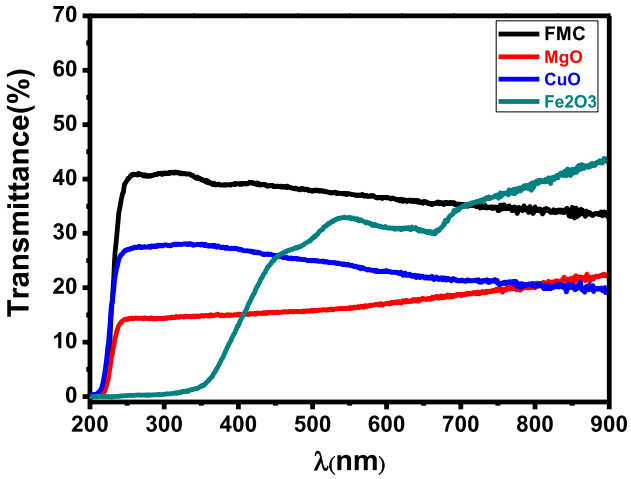

Figure 4. Transmission spectra of CuO, Fe_2O_3, MgO and Fe_2O_3–MgO–CuO (CFM) nanocomposites.

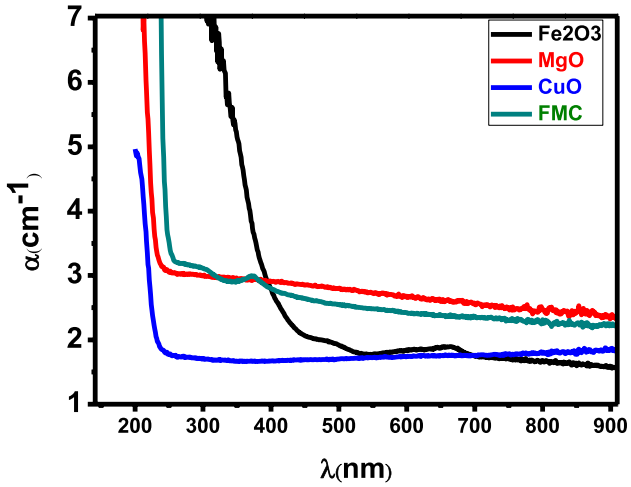

Figure 5. Absorption coefficient versus wavelength of CuO, Fe_2O_3, MgO and Fe_2O_3–MgO–CuO (FMC) nanocomposites.

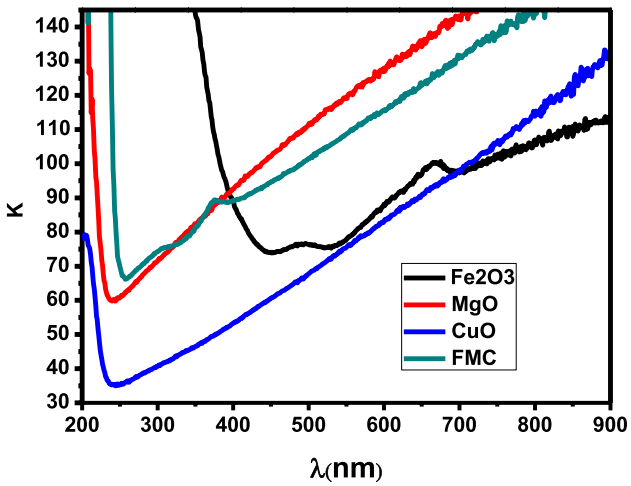

Figure 6. Extinction coefficient (k) versus wavelength of CuO, Fe_2O_3, MgO and Fe_2O_3–MgO–CuO (FMC) nanocomposites.

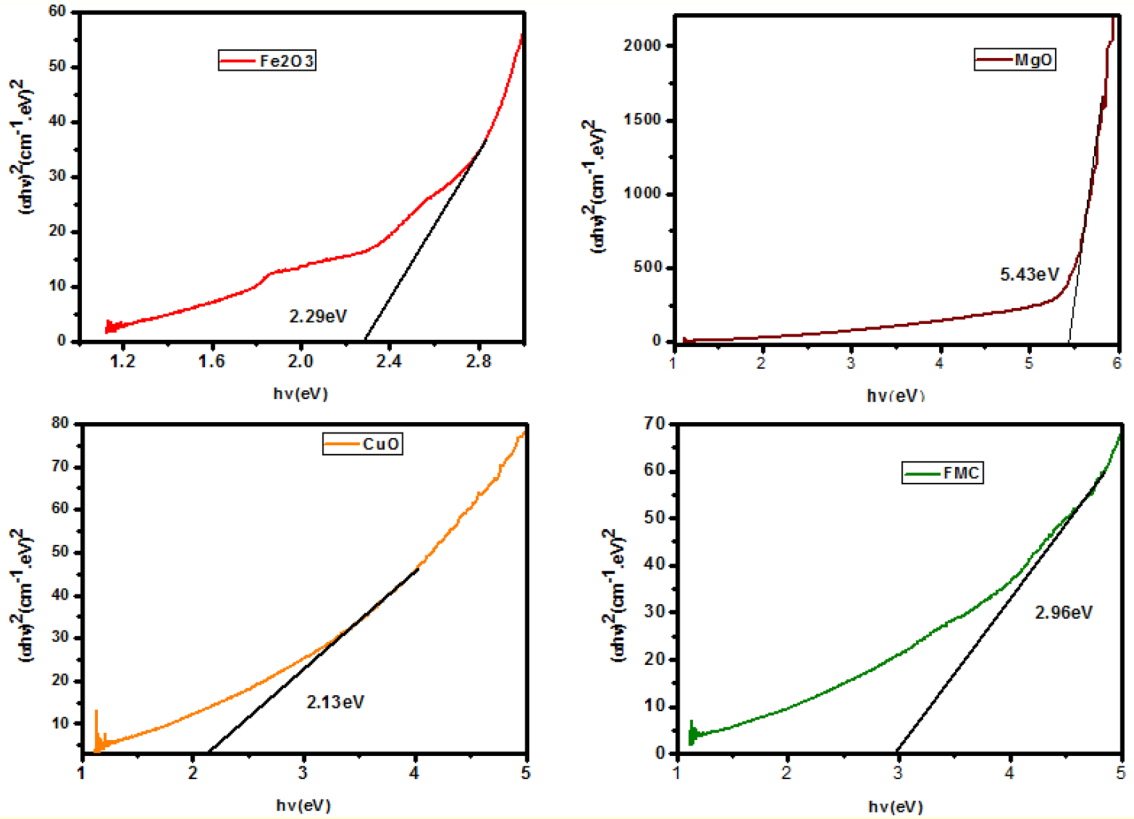

Figure 7. Optical bandgap plots for CuO, Fe_2O_3, MgO and CuO–Fe_2O_3–MgO (FMC) nanocomposite.

oxides. This can result in a shift in the electronic structure and a change in the bandgap energy. Additionally, the presence of multiple metal oxides in the NCs can also lead to increased electron–hole separation and improved charge transport properties, which can further affect the bandgap energy. This result was in good agreement with the literature[46], which showed the possibility of using the prepared materials in some optical application.

Conclusion

In Summary, tri-phase Fe_2O_3–MgO–CuO NCs and pure CuO, Fe_2O_3 and MgO NPs were successfully fabricated using a sol–gel approach. The XRD emphasized the formation of pure CuO, Fe_2O_3 and MgO NPs and CuO–Fe_2O_3–MgO NCs. The variation in the average crystallite size (D) and lattice constant were observed due to the interaction of the corresponding metal oxides. The optical bandgap was reached 2.13, 5.43, 2.29 and 2.96 eV for CuO, MgO, Fe_2O_3 and Fe_2O_3–MgO–CuO NCs, respectively.

Data availability

The datasets generated and/or analyzed during the current study are available from the corresponding author on reasonable request.

Received: 16 June 2023; Accepted: 31 July 2023
Published online: 09 August 2023

References

1. Rajeh, A., Ragab, H. M. & Abutalib, M. M. Co doped ZnO reinforced PEMA/PMMA composite: Structural, thermal, dielectric and electrical properties for electrochemical applications. *J. Mol. Struct.* **1217**, 128447 (2020).
2. Yulizar, Y., Apriandanu, D. O. B. & Jabbar, J. L. A. Facile one-pot preparation of V_2O_5–Fe_2O_3 nanocomposites using Foeniculum-vulgare extracts and their catalytic property. *Inorg. Chem. Commun.* **123**, 108320 (2021).
3. Sun, M. *et al.* Mg doped CuO–Fe_2O_3 composites activated by persulfate as highly active heterogeneous catalysts for the degradation of organicpollutants. *J. Alloys Compd.* **825**, 154036 (2020).
4. Batool, S. *et al.* Green synthesis of Cordia myxa incubated ZnO, Fe_2O_3, and Co_3O_4 nanoparticle: Characterization, and their response as biological and photocatalytic agent. *Adv. Powder Technol.* **33**, 103780 (2022).
5. Alnehia, A., Al-Sharabi, A., Al-Hammadi, A., Al-Odayni, A.-B., Alramadhan, S.A., Alodeni, R.M. Phyto-mediated synthesis of silver-doped zinc oxide nanoparticles from *Plectranthus barbatus* leaf extract: Optical, morphological, and antibacterial properties. *Biomass Convers. Bioref.* 1–13 (2023).
6. Xiang, Y. *et al.* Co_3O_4/α-Fe_2O_3 catalyzed oxidative degradation of gaseous benzene: Preparation, characterization and its catalytic properties. *Solid State Sci.* **93**, 79–86 (2019).
7. Deepthi, N. H. *et al.* Optical, electrical and luminescent studies of CuO/MgO nanocomposites synthesized via sonochemical method. *J. Alloy. Compd.* **786**, 855–866 (2019).

8. Alp, E., Eşgin, H., Kürşat Kazmanlı, M. & Genç, A. Synergetic activity enhancement in 2D CuO–Fe_2O_3 nanocomposites for the photodegradation of rhodamine B. *Ceram. Int.* **45**, 9174–9178 (2019).
9. Lei, Y., Huo, J. & Liao, H. Fabrication and catalytic mechanism study of CeO_2–Fe_2O_3–ZnO mixed oxides on double surfaces of polyimide substrate using ion-exchangetechnique. *Mater. Sci. Semicond. Process* **74**, 154–164 (2018).
10. Revathi, V. & Karthik, K. Microwave assisted CdO–ZnO–MgO nanocomposite and its photocatalytic and antibacterial studies. *Mater. Sci. Mater. Electron.* **29**, 18519–18530 (2018).
11. Amanulla, A. M. *et al.* Antibacterial, magnetic, optical and humidity sensor studies of b-CoMoO4-Co3O4 nanocomposites and its green synthesis and characterization. *J. Photochem. Photobiol. B* **183**, 233–241 (2018).
12. Vignesh, S., Muppudathi, A. L. & Sundar, J. K. Multifunctional performance of gC_3N_4–$BiFeO_3$–CuO_2 hybrid nanocomposites for magnetic separable photocatalytic and antibacterial activity. *Mater. Sci. Mater. Electron.* **31**, 13998–13999 (2020).
13. Kanwal, A., Sajjad, S., Leghari, S. A. K. & Yousaf, Z. Cascade electron transfer in ternary CuO/α-Fe_2O_3/γ-Al_2O_3 nanocomposite as an effective visible photocatalyst. *J. Phys. Chem. Solids.* **151**, 109899 (2021).
14. Hammood, S. A. *et al.* Synthesis and characterization of PVA–Fe_2O_3–CuO hybrid structure for biomedical application. *Int. J. Nanosci.* **21**, 2250030 (2022).
15. Rahmah, M. I. Novel triple hydrothermal method for preparation of CuO/Fe_2O_3/Ag_2O nanocomposite with antimicrobial application. *Inorg. Nano-Metal Chem.* (2023).
16. Hong, Z., Cao, Y. & Deng, J. A convenient alcohothermal approach for low temperature synthesis of CuO nanoparticles. *Mater. Lett.* **52**, 34–38 (2002).
17. Selvi, K. T., Mangai, K. A., Priya, M. & Sagadevan, S. Enhanced electrical and magnetic properties of CuO/MgO nanocomposites. *Chem. Phys. Lett.* **765**, 138320 (2021).
18. Grigore, M. E., Biscu, E. R., Holban, A. M., Gestal, M. C. & Grumezescu, A. M. Methods of synthesis properties and biomedical applications of CuO nanoparticles. *Pharmaceuticals* **9**, 75 (2016).
19. Munawar, T. *et al.* Sunlight-induced photocatalytic degradation of various dyes and bacterial inactivation using CuO–MgO–ZnO nanocomposite. *Environ. Sci. Pollut. Res.* **28**, 42243–42260 (2021).
20. Khodair, Z. T., Al-Saadi, T. M., Abed, A. H. Effect of fuel on the structural and optical properties of MgO nanoparticles prepared by auto-combustion of sol–gel method. *Adv. Phys. Theories Appl.* **60** (2016).
21. Dinga, E. *et al.* Phyto-me diate d synthesis of MgO nanoparticles using Melia azedarach seed extract: Larvicidal and antioxidant activities. *Sci. Afr.* **17**, e01366 (2022).
22. Al-Sharabi, A., Sada'a, K. S., Al-Osta, A. & Abd-Shukor, R. Structure, optical properties and antimicrobial activities of MgO–Bi2– x Cr x O3 nanocomposites prepared via solvent-deficient method. *Sci. Rep.* **12**, 10647 (2022).
23. Ramesh, R. *et al.* Biogenic synthesis of α-Fe_2O_3 nanoparticles using *Plectranthus amboinicus* leaf extrac. *Mater. Today Proc.* **36**, 453–458 (2020).
24. Alam, M. M. *et al.* Fabrication of ascorbic sensor acid with Co_3O_4 Fe_2O_3 nanosphere materials by electrochemical technique. *Surf. Interfaces* **20**, 100607 (2020).
25. Bin Ren, J. M. *et al.* A grape-like N-doped carbon/CuO-Fe_2O_3nanocomposite as a highly active heterogeneous Fenton-like catalyst in methylene blue degradation. *J. Clean. Prod.* **240**, 118143 (2019).
26. Shekoohiyan, S. *et al.* A novel CuO/Fe_2O_3/ZnO composite for visible-light assisted photocatalytic oxidation of Bisphenol A: Kinetics, degradation pathways, and toxicity elimination. *Sep. Purif. Technol.* **242**, 116821 (2020).
27. Zhuang, Y. *et al.* Co_3O_4–CuO hollow nanocage hybrids with high oxidase-like activity for biosensing of dopamine. *Mater. Sci. Eng. C* **C94**, 858–866 (2019).
28. Subhan, M. A., Uddin, N., Sarker, P., Azad, A. K. & Begum, K. Photoluminescence, photocatalytic and antibacterial activities of Ce_O2–CuO–ZnO nanocomposite fabricated by co-precipitation method. *Spectrochim. Acta* **149**, 839–850 (2015).
29. Kulkarni, J. *et al.* Structural optical and photocatalytic properties of MgO/CuO nanocomposite prepared by a solution combustion method. *Mater. Today Proc.* **4**, 11756–11763 (2017).
30. Karthik, K., Dhanuskodi, S., Gobinath, C., Prabukumar, S. & Sivaramakrishnan, S. Ultrasonic-assisted CdO–MgO nanocomposite for multifunctional applications. *Mater. Technol.* **34**, 403–414 (2019).
31. Alnahari, H., Al-Sharabi, A., Al-Hammadi, A., Al-Odayni, A.-B. & Alnehia, A. Synthesis of glycine-mediated CuO–Fe_2O_3–MgO nanocomposites: Structural, optical, and antibacterial properties. *Compos. Adv. Mater.* **32**, 1–13 (2023).
32. Lermusiaux, L., Mazel, A., Carretero-Genevrier, A., Sanchez, C. & Drisko, G. L. Metal-induced crystallization in metal oxides. *Acc. Chem. Res.* **55**, 171–185 (2022).
33. Munawar, T., Iqbal, F., Yasmeen, S., Mahmood, K. & Hussain, A. Multi metal oxide NiO–CdO–ZnO nanocomposite-synthesis, structural, optical, electrical properties and enhanced sunlight driven photocatalytic activity. *Ceram. Int.* **46**, 2421–2437 (2020).
34. Alnehia, A., Al-Hammadi, A., Al-Sharabi, A. & Alnahari, H. Optical, structural and morphological properties of ZnO and Fe+ 3 doped ZnO-NPs prepared by *Foeniculum vulgare* extract as capping agent for optoelectronic applications. *Inorg. Chem. Commun.* **143**, 109699 (2022).
35. Alnahari, H., Al-Hammadi, A. H., Al-Sharabi, A., Alnehia, A. & Al-Odayni, A.-B. Structural, morphological, optical, and antibacterial properties of CuO–Fe_2O_3–MgO–$CuFe_2O_4$ nanocomposite synthesized via auto-combustion route. *J. Mater. Sci. Mater. Electron.* **34**, 682 (2023).
36. Al-Ariki, S. *et al.* Synthesis and comparative study on the structural and optical properties of ZnO doped with Ni and Ag nanopowders fabricated by sol gel technique. *Sci. Rep.* **11**, 11948 (2021).
37. Alnehia, A. *et al.* Garlic extract-mediated synthesis of ZnS nanoparticles: Structural optical, antibacterial and hemolysis studies. *Nanomaterials* **2023**, 1–9 (2023).
38. Al-Sharabi, A., Alnehia, A., Al-Hammadi, A. H., Alhumaidha, K. A. & Al-Osta, A. The effect of Nigella sativa seed extract concentration on crystal structure, band gap and antibacterial activity of ZnS-NPs prepared by green route. *J. Mater. Sci. Mater. Electron.* **33**, 20812–20822 (2022).
39. Abutalib, M. M. & Rajeh, A. Enhanced structural, electrical, mechanical properties and antibacterial activity of Cs/PEO doped mixed nanoparticles (Ag/TiO_2) for food packaging applications. *Polym. Test.* **93**, 107013 (2021).
40. Zhou, W. & Greer, H. F. What can electron microscopy tell us beyond crystal structures?. *Eur. J. Inorg. Chem.* **2016**, 941–950 (2016).
41. Jensen, H. *et al.* Determination of size distributions in nanosized powders by TEM, XRD, and SAXS. *J. Exp. Nanosci.* **1**, 355–373 (2006).
42. Al-Osta, A., Alnehia, A., Qaid, A. A., Al-Ahsab, H. T. & Al-Sharabi, A. Structural, morphological and optical properties of Cr doped ZnS nanoparticles prepared without any capping agent. *Optik Int. J. Light Electron Opt.* **214**, 164831 (2020).
43. Al-Sharabi, A., Alnehia, A., Al-Osta, A. & Yahya, N. A. A. Effect of copper doping on structural and optical properties of zinc sulfide (ZnS) nanoparticles. *Al-Baydha Univ. J. Res.* **1**, 224–234 (2019).
44. Alwany, A. B. *et al.* Structural, optical and radiation shielding properties of ZnS nanoparticles. *QDs Optik Int. J. Light Electron Opt.* **260**, 169124 (2022).
45. Mukhtar, F. *et al.* Dual S-scheme heterojunction ZnO–V_2O_5–WO nanocomposite with enhanced photocatalytic and antimicrobial activity. *Mater. Chem. Phys.* **263**, 124372 (2021).
46. Rahman, A. *et al.* Structural, optical and photocatalytic studies of trimetallic oxides nanostructures prepared via wet chemical approach. *Synth. Met.* **259**, 116228 (2020).

Acknowledgements
The authors are grateful to Mr. Ahmed Al-Khalaki for the help with optical experiments.

Author contributions
Conceptualization: H.A., A.A.-S. and A.H.A.-H. Methodology: A.A. and H.A. Formal analysis and investigation: A.A., H.A., A.A.-S. and A.H.A.-H. Writing—original draft: H.A., A.A. and A.A.-S. Writing-review and editing: A.-B.A.-O., A.A., and A.A.-S. Visualization: A.A., H.A. and A.-B.A.-O. Supervision: A.A.-S. and A.H.A.-H.

Competing interests
The authors declare no competing interests.

Additional information
Correspondence and requests for materials should be addressed to H.A.

Reprints and permissions information is available at www.nature.com/reprints.

Publisher's note Springer Nature remains neutral with regard to jurisdictional claims in published maps and institutional affiliations.